7524 *J. Phys. Chem. A* **2003,** *107,* 7524−7538

Structure of Solvated $Fe(CO)_5$: FTIR Measurements and Density Functional Theory Calculations

Yan Jiang, Taewoo Lee, and Christoph G. Rose-Petruck*

Department of Chemistry, Box H, Brown University, Providence, Rhode Island 02912

Received: October 18, 2002; In Final Form: May 28, 2003

The structure of iron pentacarbonyl, $Fe(CO)_5$, solvated in various solvents has been investigated by FTIR measurements and density functional theory (DFT) calculations. The primary focus rested on the solvation properties of iron pentacarbonyl in aromatic solvents ranging from benzene to increasingly fluorinated derivatives. While, in the gas phase, most iron pentacarbonyl molecules have D_{3h} symmetry, about 60−90% of them have C_{2v} or C_{4v} symmetry in aromatic solvents at room temperature. The C_{4v} structure exists in the gas phase as a transition state during a Berry pseudorotation. In solution, this transition state is stabilized by interaction with a solvent molecule located trans to the apical ligand of $Fe(CO)_5(\sim C_{4v})$, forming a weakly interacting solute−solvent complex. Benzene, for instance, does not coordinate to the iron with its π-system but with one of its aryl hydrogens. The equilibrium populations of conformers with various symmetries were investigated through (i) calculations of the Gibbs free energy for D_{3h}, C_{2v}, and C_{4v} conformers of $Fe(CO)_5$ after DFT structure refinement of the $Fe(CO)_5$−solvent complex, (ii) experimental FTIR data in combination with theoretical IR absorption intensity values from our DFT calculations, and (iii) entirely experimental temperature-dependent FTIR data. The configuration population measurements relied on an absorption band around 2113 cm^{-1}, which was assigned to a CO-stretching vibration of C_{2v} and C_{4v} symmetry. While this stretching mode is exclusively Raman active in D_{3h} symmetry, it becomes increasingly IR active as the symmetry of $Fe(CO)_5$ is broken by solvation. The absorption band is about a factor 800 weaker than the ones around 2000 cm^{-1}, which are usually considered in IR spectroscopy of CO vibrations. We demonstrate that, despite its small intensity, this mode carries quantitative spectroscopic information about the conformer distribution.

1. Introduction

Transition metal carbonyls play an important role in many areas such as organometallic syntheses, catalysis, biological processes, and materials chemistry.[1−6] Their chemical dynamics has been studied in the gas and liquid phases by static or time-resolved methods.[7−16] Hexacoordinated single metal carbonyls, such as a $Cr(CO)_6$, are structurally rather rigid. It can be expected that their symmetries change little upon solvation. In contrast, pentacoordinated complexes, such as $Fe(CO)_5$, are fluxional, enabling ligands to rapidly exchange positions. Such ligand motions cause temporary changes of the molecular symmetry.[5,6] It is generally accepted that the theoretically most stable geometry for $Fe(CO)_5$ and other d^8 systems is the trigonal bipyramid.[17,18] This configuration has been confirmed by X-ray diffraction[19] and electron diffraction measurements.[20−22] Nevertheless, for $Fe(CO)_5$ this D_{3h} structure has only slightly lower energy than the square pyramidal structure C_{4v}. In fact, several d^8 systems that exhibit D_{3h} as well as C_{4v} conformation are known.[23−27] For instance, the X-ray crystal structure of $Ni(CN)_5^{3-}$ shows the simultaneous existence of one C_{4v} conformer and one conformer with symmetry between D_{3h} and C_{4v}.[24] The conversion of $Fe(CO)_5$ from D_{3h} to C_{4v} conformation has been calculated to require an energy between 0.6 kcal/mol[17,28] and 2.3 kcal/mol.[29] This small energy barrier enables iron pentacarbonyl (IPC) to undergo Berry pseudorotation,[30] that is, a deformation of the ground-state symmetry from D_{3h} into C_{2v} and on to the C_{4v} transition state. From there, the deformation continues to a 90° rotated C_{2v} and finally a D_{3h} structure. This effect was first observed in PF_5.[30] In the thermodynamic equilibrium, the C_{4v} transition state and the D_{3h} ground-state populations of $Fe(CO)_5$ can be calculated to theoretically range from 1.4% to 25%. These calculated populations are, of course, sensitively dependent upon the Gibbs free energy values used to calculate the equilibrium constant, which can be expected to change upon solvation. On the basis of NMR measurements Spiess et al.[31] estimated the lifetime for each configuration in liquid IPC at 250 K to be between 10 and 90 ps. These authors measured a 1 kcal/mol energy barrier for pseudorotation in solution. It is clear that in equilibrium a substantial amount of isolated $Fe(CO)_5$ molecules may be in the C_{4v} configuration. Although the existence of the C_{2v} and C_{4v} structures has long been recognized, few studies have investigated these conformers.[32−34] Furthermore, the small energy barrier suggests that the conformer distribution should be sensitive to solvation. Here, we show that $Fe(CO)_5(C_{2v})$ is the dominant conformer in aromatic solvents. While even a slight deformation of the D_{3h} geometry formally generates a C_{2v} structure, the molecular deformations discussed here are substantial. In fact, $Fe(CO)_5(C_{2v})$ assumes nearly C_{4v} symmetry with a solvent molecule directly interacting with the iron center. In the resulting IPC−solvent (IPC−S) complex, the solvent molecule is located trans to the apical ligand of $Fe(CO)_5(\sim C_{4v})$. Such a complex exhibits specific IR active bands that are nonexistent in $Fe(CO)_5(D_{3h})$. We use FTIR measurements in combination with density functional theory (DFT) calculation in order to measure the relative concentration and structure of the IPC−S complex in various aromatic solvents.

Solvated $Fe(CO)_5$ has been spectroscopically investigated for decades, and the CO stretching modes of $Fe(CO)_5$ with D_{3h}

---

* Corresponding author. Phone: (401) 863-1533. Fax: (401) 863-2594. E-mail address: Christoph_Rose-Petruck@brown.edu.

10.1021/jp0272522 CCC: $25.00 © 2003 American Chemical Society
Published on Web 08/29/2003

symmetry are well-known.[35-42] In solution, prominent absorption peaks appear between 1967 and 2034 cm^{-1}. Assuming a D_{3h} symmetry of IPC, these peaks correspond to the IR active CO stretching modes $\nu_{10}(E')$ and $\nu_6(A_2'')$.[41-49] They are generally red-shifted relative to the gas-phase peaks and, depending on the solvent, are more or less broadened. These absorption peaks are, however, not very symmetry sensitive, as bands in this spectral range exist for D_{3h} as well as for C_{2v} and C_{4v} structures. While lowering the symmetry lifts the degeneracy of the largest peak (with E′ symmetry), peak broadening generally obscures any interpretable change of the absorption band shape. In contrast, at larger vibrational energies between 2050 and 2200 cm^{-1}, weak IR absorption lines exist, which are strongly symmetry sensitive. Most of the absorption bands are combination bands. However, the ν_1 normal mode at about 2115 cm^{-1} is Raman but not IR active for $Fe(CO)_5(D_{3h})$. It becomes IR active for $Fe(CO)_5(C_{2v},C_{4v})$ due to the conformer's reduced symmetry. This is in general agreement with the fact that pentacoordinated metal complexes of the form MA_4B and C_{4v} configuration have three IR active bands in the CO stretching region, one of which lies above 2100 cm^{-1}.[50] For instance, iron carbonyls with C_{4v} symmetry, such as ax-$Fe(CO)_4PF_3$, have CO stretching bands at 1993 cm^{-1} (E), 2028 cm^{-1} (A_1), and 2092 cm^{-1} (A_1).[46] The A_1 modes of other carbonyls with C_{4v} symmetry, such as $Mn(CO)_5I$, $Re(CO)_5Cl$, and $Mo(CO)_5Py$, are at higher frequencies.[51-53] Chemisorbed iron pentacarbonyl has A_1 modes at 2010 and 2064 cm^{-1}.[34] Slightly distorting IPC with C_{4v} symmetry reduces its symmetry to C_{2v}. Metal pentacarbonyls with C_{2v} symmetry have four IR active bands, one of B_1, one of B_2, and two of A_1 symmetries. For instance, eq-$Fe(CO)_4PF_3$ has IR bands at 1999 (B_1), 2018 (B_2), 2022 (A_1), and 2101 (A_1) cm^{-1}.

The relative populations for the IPC conformers with D_{3h}, C_{2v}, and C_{4v} symmetry solvated in benzene and its fluorinated derivatives were determined from Gibbs free energy values obtained by three different methods. We used (i) calculations of the values of thermodynamic state functions for D_{3h}, C_{2v}, and C_{4v} conformers of IPC after structure refinement of the IPC−S complex using density functional theory calculations, (ii) measurements of FTIR spectra for IPC solvated in aromatic solvents and quantitative spectral analysis in combination with theoretical integral IR absorption coefficients from our DFT calculations, and (iii) quantitative analysis of experimental temperature-dependent FTIR spectra without any computational input. The goal of this work is the determination of the equilibrium conformer distribution of solvated iron pentacarbonyl, thereby providing support for static[54,55] and time-resolved X-ray absorption studies with our recently developed high repetition rate ultrafast X-ray source.[56-58]

2. Computational Details and Results

Initially, semiempirical calculations were performed for one $Fe(CO)_5$ in clusters of typically 10 solvent molecules in order to get an approximate model for the structure of the solute and its first solvation shell. All calculations were performed with the Jaguar package.[59] The semiempirical calculations were carried out with a PM3 basis function set. The initial solvent positions relative to the solute were randomly selected. The energy of the cluster was subsequently minimized as the molecular distances and orientations were permitted to freely change. Clearly, this level of theory is not sufficient for reliable determination of the solvation energies or the normal mode frequencies and IR absorption strengths. Nevertheless, the result demonstrates that $Fe(CO)_5$ changes its conformation to C_{2v} or C_{4v} and interacts with a solvent molecule trans to the apical ligand, as depicted in Figure 1 for a benzene solvent cluster. The apical ligand is slightly angled. The IPC−S complex structure is very little influenced by surrounding solvent molecules, and after extensive calculations of IPC in various solvent clusters, we concluded that calculations of just the IPC−S complex capture most of the essential properties of the solvation structure while permitting higher level theoretical calculations on the density functional level of theory.

DFT calculations of the IPC−S complex were carried out for benzene (Bz) and pentafluorobenzene (PFBz). Our goal was to calculate the vibrational frequencies and IR absorption intensities for the IPC−S complex as well as estimates of its thermodynamic properties at various distances between the iron and the closest hydrogen atom in the Bz and PFBz. The total energy of the IPC−S complex was minimized under the constraints of various benzene hydrogen−iron distances decreasing from 330 to 200 pm. These calculations yielded the complex's energy profile and its equilibrium geometries along this specific reaction coordinate. Three representative geometries of the IPC−S complex were considered for further analysis. They correspond to IPC−S distances of 330, 225, and 200 pm and are depicted as structures 1, 2, and 3 in Chart 1. The displayed structural data are in good agreement with literature data.[29] At these distances, the symmetry of $Fe(CO)_5$ changes from nearly perfect D_{3h} to C_{2v} and finally to a slightly broken C_{4v} symmetry. At close IPC−Bz distances, the σ_h plane of the benzene intersects with IPC nearly symmetrically between the CO ligands, resulting in an overall C_{2v} symmetry of the IPC−S complex; see structure 3 of Chart 1. In contrast, at 330 pm the solute−solvent interaction was found to be very small, resulting in little deviation from the D_{3h} symmetry. For these and intermediate structures, we calculated the respective thermodynamic properties in order to obtain the change in Gibbs free energy between the nearly perfect D_{3h} geometry, various C_{2v} geometries, and the nearly perfect C_{4v} geometry. The nearly D_{3h} structure is in good agreement with other theoretical and experimental structure data.[19,20,29] One might expect the interaction of IPC with the π-electrons of benzene. However, the calculations show that the interaction occurs through a CH group. Moreover, the CH bond lengths increase as the distance between IPC and the aryl hydrogen decreases. Simultaneously, electron density shifts from the metal center to the aryl hydrogen and the Fe−H−C bond path straightens. This indicates that benzene interacts with IPC through a hydrogen bond. Fluorinated derivatives of benzene might interact in an angled configuration. We are currently investigating this theoretically and experimentally.

2.1. Calculation of Vibrational Frequencies and IR Absorption Intensities. The intensity of the ν_1 peak, relative to the bands around 2000 cm^{-1} is about 0.1% or less. This seems to suggest that it is of minor importance for the structural analysis of solvated IPC. However, the theoretical IR absorption intensity is about 3 orders of magnitude smaller than that of the big peaks due to the high symmetry of the corresponding normal mode. Thus, the small absorption strength of this peak in solution is not indicative of a small population in the corresponding conformation. Furthermore, the appearance of this peak requires non-D_{3h} symmetry. Consequently, we used its intensity as a measure of the relative population of non-D_{3h} conformers of solvated IPC. Our related FTIR measurements and the quantitative spectral analysis are described in section 3.

To calculate IR spectra of the solvated iron pentacarbonyl, the normal mode frequencies along with their integral IR

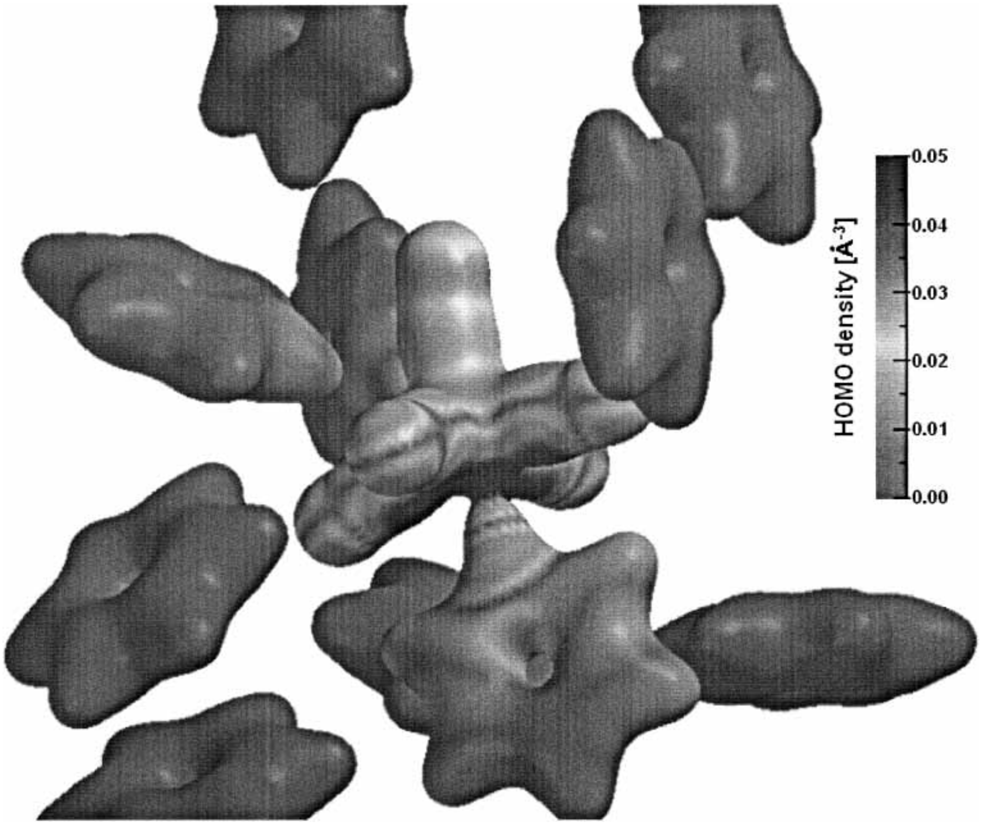

Figure 1. Typical result of a semiempirical quantum calculation of the minimum-energy structure of $Fe(CO)_5$ solvated by 10 benzene molecules. The electron density isosurface (0.05 electrons/Å^3) is shown. The magnitude of the HOMO is mapped onto the isosurface with dark gray depicting low and lighter gray depicting high orbital density. Note the substantial distortion of $Fe(CO)_5$.

CHART 1: Representative IPC−Bz Structures at Various Solute−Solvent Distances in Picometers

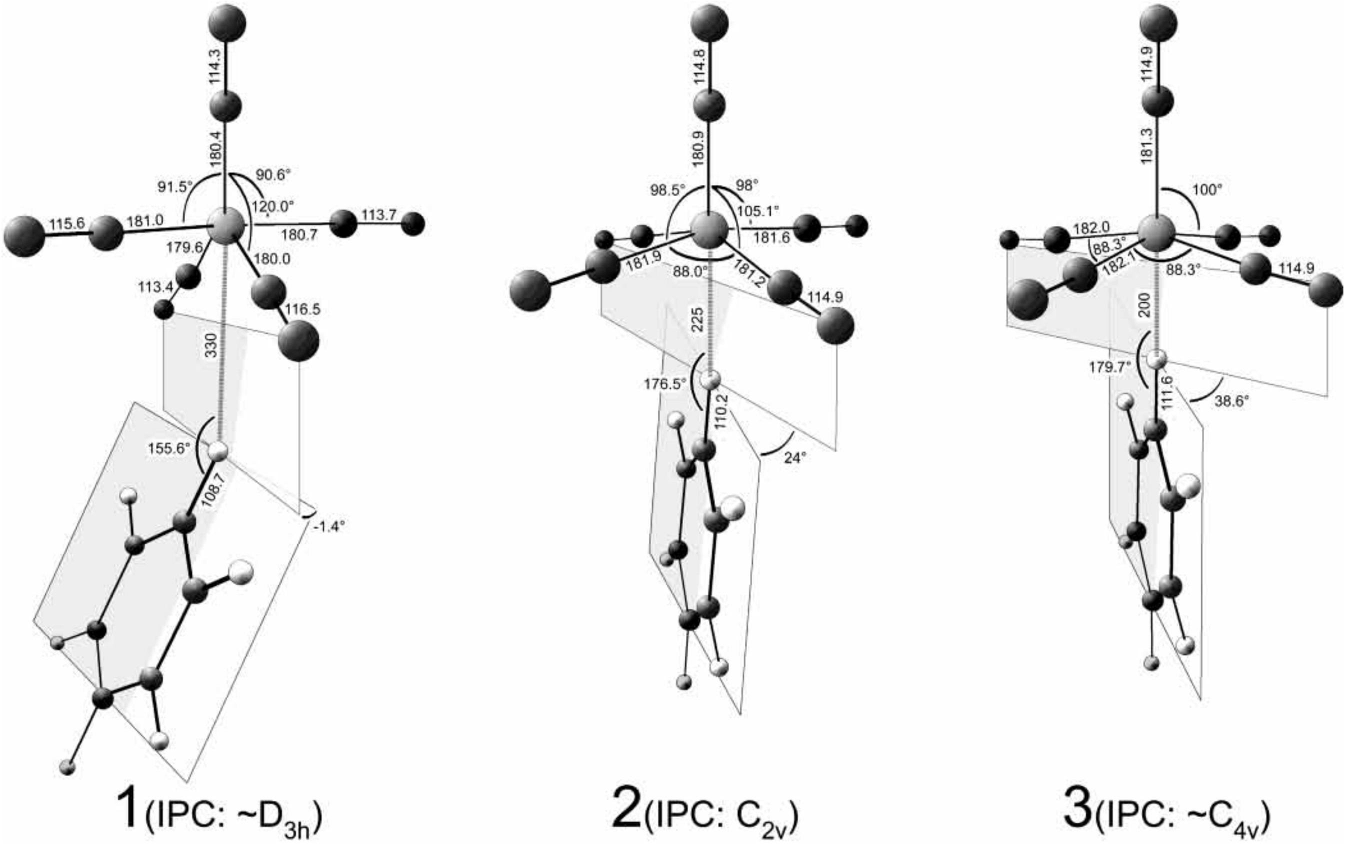

absorption coefficients were calculated for the perfect D_{3h} geometry, the C_{4v} geometry, and several C_{2v} geometries; they are displayed in Table 1. To obtain a reasonable approximation of the IPC geometry at various IPC−S distances, we first

TABLE 1: Theoretical Vibrational Frequencies and Absorption Intensities of IR Active Bands of Iron Pentacarbonyl in D_{3h}, C_{4v}, and C_{2v} Symmetries

IPC−S structure		M$_1$[a]		M$_2$[b]	M$_3$[c]	M$_4$[d]	M$_1$/(M$_2$ + M$_3$)	M$_1$ + M$_2$ + M$_3$	M$_4$/(M$_1$ + M$_2$ + M$_3$)
D_{3h} from	frequency (cm^{-1})	2067	2067	2093	2094	2169			
ref 29	integrated absorb coeff (km/mol)	1274	1274	0	1474	0	1.73	4022	0.000%
D_{3h}	frequency (cm^{-1})	2097.47	2097.47	2124.49	2125.84	2193.1			
	int abs coeff (km/mol)	1119	1118	0	1321	0	1.69	3558	0.000%
330 pm	frequency (cm^{-1})	2092.19	2094.45	2121.21	2125.41	2190.57			
	int abs coeff (km/mol)	1109	1125	81	1238	0	1.69	3553	0.012%
275 pm	frequency (cm^{-1})	2084.26	2093.13	2118.98	2122.09	2188.1			
	int abs coeff (km/mol)	1164	1034	44	1323	1	1.61	3564	0.030%
250 pm	frequency (cm^{-1})	2092.93	2102.12	2120.15	2125.95	2191.84			
	int abs coeff (km/mol)	1301	791	915	548	4	1.43	3554	0.118%
225 pm	frequency (cm^{-1})	2098.82	2109.93	2112.91	2123.76	2189.51			
	int abs coeff (km/mol)	1236	1156	526	595	7	2.14	3513	0.190%
200 pm	frequency (cm^{-1})	2103.55	2105.08	2112.3	2114.56	2186.61			
	int abs coeff (km/mol)	1318	1366	95	754	5	3.16	3533	0.141%
C_{4v}	frequency (cm^{-1})	2102.94	2102.94	2110.88	2118.53	2185.7			
	int abs coeff (km/mol)	1320	1329	0	840	4	3.15	3489	0.120%
C_{4v} from ref 29	frequency (cm^{-1})	2075	2075	2081	2086	2166			
	int abs coeff (km/mol)	1510.5	1510.5	0	979	1	3.09	4000	0.025%

[a] Mode corresponds to $\nu_{10}(D_{3h})$ and $\nu_4(C_{2v}$ and $C_{4v})$. [b] Mode corresponds to $\nu_2(D_{3h})$ and $\nu_3(C_{2v}$ and $C_{4v})$. [c] Mode corresponds to $\nu_6(D_{3h})$ and $\nu_2(C_{2v}$ and $C_{4v})$. [d] Mode corresponds to $\nu_1(D_{3h}$, C_{2v}, and $C_{4v})$.

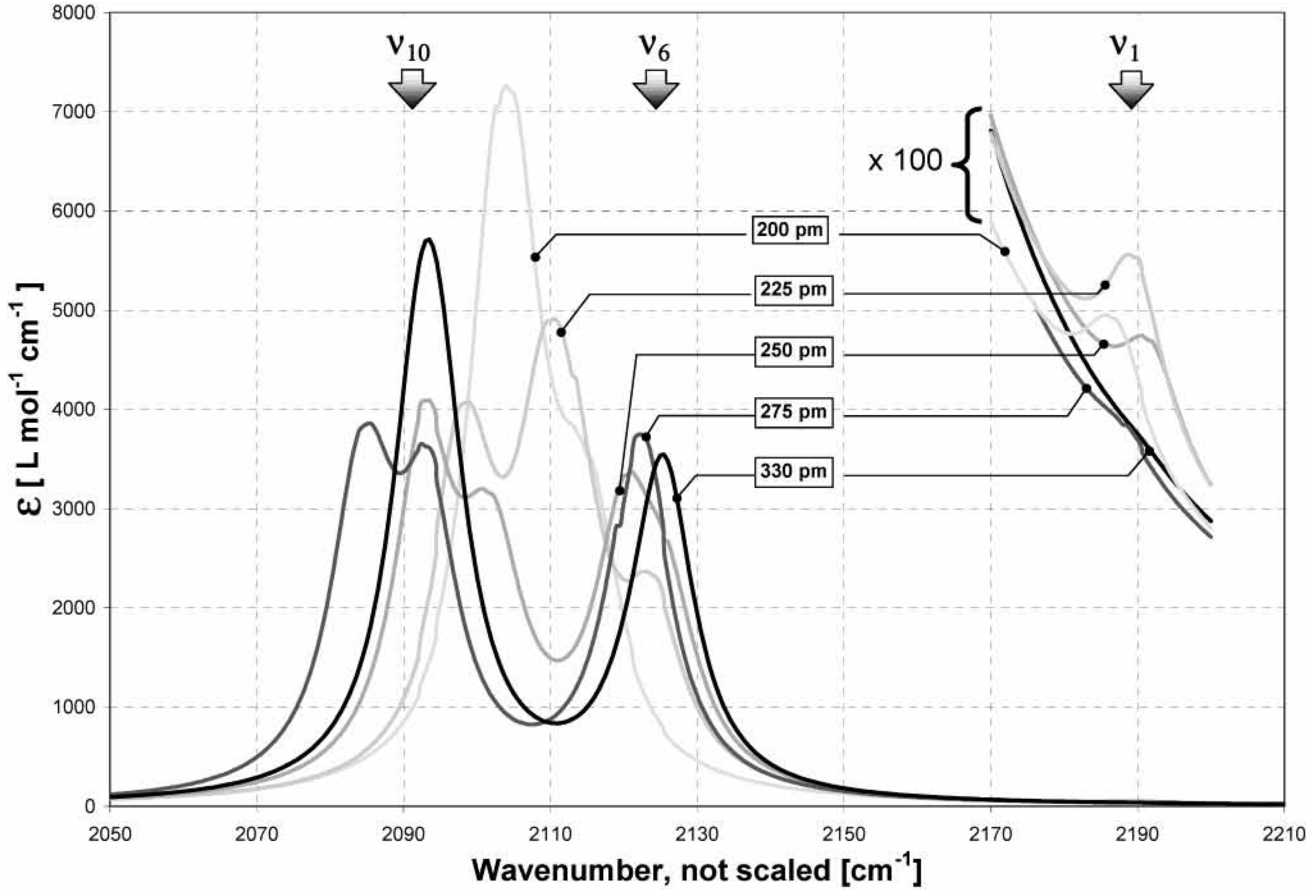

Figure 2. Theoretical IR absorption spectrum of IPC at various IPC−Bz complex distances. In this and all other spectra, the mode labels for D_{3h} symmetry were used to identify peaks. This does not imply that the spectra shown should only be assigned to the D_{3h} confromer.

energy-minimized the structure of an IPC−benzene (IPC−Bz) complex under the constraint of the desired IPC−Bz distance, specifically the distance between the IPC iron atom and the closest hydrogen atom in benzene. Then, the benzene was removed from the obtained complex and the positions of all IPC atoms were frozen. Finally, the IPC single-point energy was recalculated under these constraints. This procedure yielded an IPC geometry that was subsequently used to calculate the desired IR parameters. The corresponding spectra, displayed in Figure 2, were obtained through convolution of the calculated mode frequencies with a Lorentzian peak shape with 10 cm^{-1} (fwhm). The displayed spectra are not scaled, and the peak centers are typically 100 cm^{-1} larger than the experimental values. The intensity of the ν_1 mode relative to the sum of the intensities of the ν_6 and ν_{10} modes is displayed in Figure 3 for various IPC−S distances. While our calculated IR absorption strengths for the ν_6 and ν_{10} modes are in good agreement with literature data, our values for the ν_1 mode are about 4 times

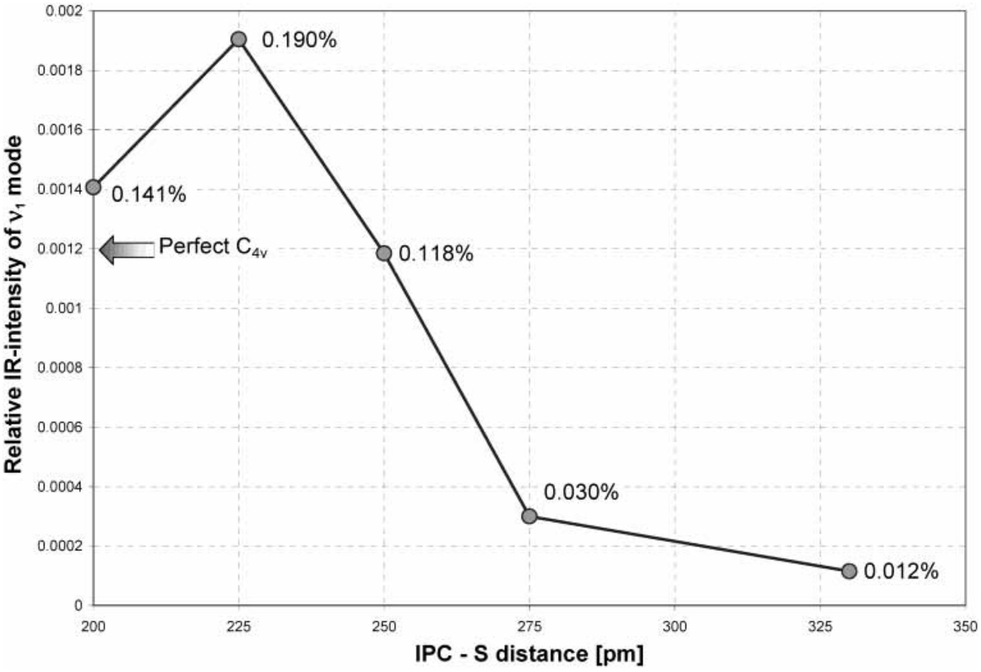

Figure 3. Theoretical relative integrated IR intensities of the ν_1 mode of IPC at various IPC−Bz complex distances. The intensities are measured relative to the integrated intensities of the large ν_6 and ν_{10} peaks as displayed in Figure 2.

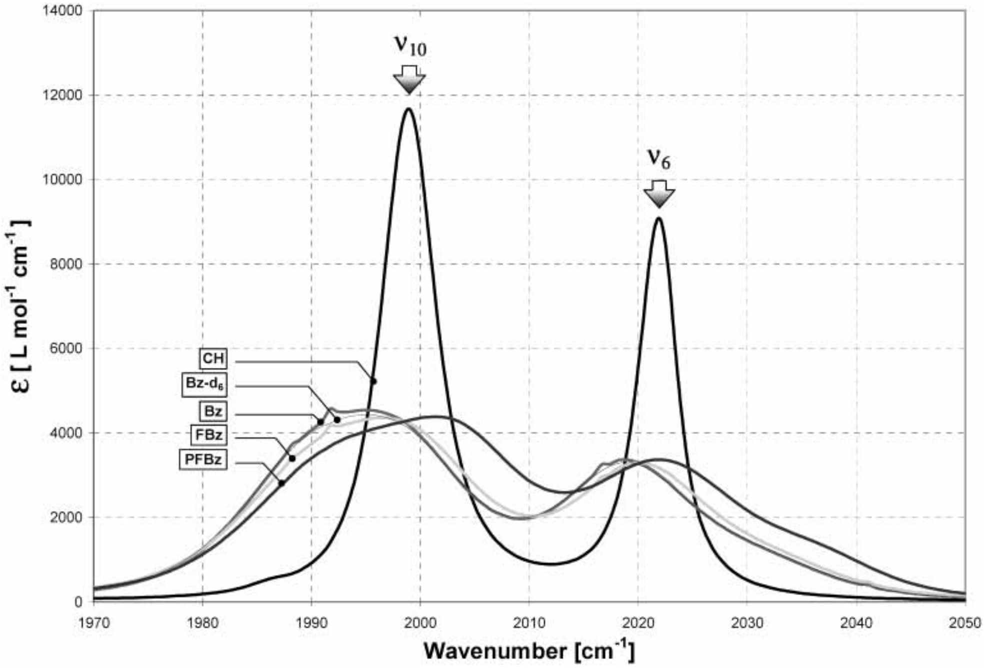

Figure 4. FTIR spectra of 10 mM iron pentacarbonyl in cyclohexane, deuterated benzene, benzene, fluorobenzene, and pentafluorobenzene.

larger.[29] We believe that our calculation results are more realistic because, upon normalization of our measured IR spectra with the calculated IR absorption strengths, we obtain reasonable populations for conformers with D_{3h} and C_{4v} or lower symmetries. In contrast, using the literature values yielded the obviously incorrect result of over 100% in the C_{2v} conformation.

TABLE 2: Fit Results of the Measured FTIR Spectra of IPC in Cyclohexane, Benzene, Fluorobenzene, and Pentafluorobenzene[a]

	IPC−S distance (pm)					IR energy scale		average quantities	
solvent	330	275	250	225	200	multi-plier	offset ($\mathrm{cm^{-1}}$)	IPC−S dist (pm)	ν_1 rel int
CH	100%	0%	0%	0%	0%	1.436	−94.586	330	0.012%
Bz	16%	0%	66%	3%	15%	0.961	−102.944	254	0.107%
FBz	9%	0%	70%	5%	16%	0.914	−102.538	248	0.116%
PFBz	0%	0%	66%	13%	21%	0.831	−101.233	236	0.132%

[a] The uncertainties of the fitted conformer populations are about 10%.

The theoretical spectra were fitted to the experimental spectra, displayed in Figure 4, to obtain an estimate for the equilibrium distribution of IPC−S distances at room temperature. The fit results are listed in Table 2 along with their respective wavelength scale multipliers and offsets. These distributions were subsequently used to estimate the equilibrium IPC−S distances and average ν_1 relative intensities which are listed in the last columns of Table 2. These results were later used for normalization of peak areas of the measured FTIR spectra. Columns 7 and 8 of Table 2 list the offset and multiplier values used to scale the theoretical wavelength scale to the experimental scale according to the formula

$$\nu_{\text{exp}} = \text{multiplier}(\nu_{\text{theor}} - 2000\ \text{cm}^{-1} - \text{offset}) + 2000\ \text{cm}^{-1} \quad (1)$$

The multiplier value for IPC−Bz is expected for the DFT calculation carried out. However, the variations of multiplier and offset values indicate that at each IPC−S distance the electronic structure of IPC, for instance, in cyclohexane (CH) differs from that in benzene, resulting in different normal mode frequencies. This, of course, is expected, as the ν_1 mode is nearly absent, which implies a nearly undisturbed D_{3h} symmetry of IPC. Furthermore, the experimental peaks for fluorobenzene and pentafluorobenzene were fitted using the theoretical structures for benzene. While we claim that IPC will be primarily in the C_{2v} conformation in the aromatic solvents used, we do not claim that the structures in the fluorinated benzene derivatives are identical to that in benzene. Structural differences are suggested by the fact that the spectral multipliers and offsets deviate substantially from those expected for this level of theory. It is, for instance, conceivable that the Fe−H−C bond path is not straight in benzene derivatives. We are currently investigating the structures in these systems in more detail.

2.2. Calculation of Thermodynamic Quantities. Using the normal mode frequency spectrum, we calculated thermodynamic data at various IPC−S distances. Since IPC assumes nearly perfect D_{3h} symmetry at an IPC−S distance of 330 pm, we chose the Gibbs free energy at this distance as the energy reference point. Evaluating the conformer distribution of IPC−S at room temperature required the calculation of changes of the enthalpy ΔH_{298}, the entropy ΔS_{298}, and the Gibbs free energy ΔG_{298} upon reduction of the solute−solvent distances and change of the IPC−S conformation. Thus, the Gibbs free energy change ΔG_{298} at 298 K as a function of distance is

$$\Delta G_{298} = G(\text{IPC}-\text{S distance}) - G(330\ \text{pm}) = G - G^\circ = \Delta H_{298} - T\Delta S_{298}$$

with

$$\Delta H_{298} = H(\text{IPC}-\text{S distance}) - H(330\ \text{pm}) = H - H^\circ + \text{BSSE}$$

$$\Delta S_{298} = S(\text{IPC}-\text{S distance}) - S(330\ \text{pm}) = S - S^\circ \quad (2)$$

BSSE refers to the basis set superposition error discussed below. The superscripts denote thermodynamic functions calculated at the largest solute−solvent distance (330 pm) considered. Thus, positive quantities indicate increasing values for decreasing distances. The enthalpy change ΔH at $T = 298$ K consists of the difference in complex energies D_e, the difference in zero point vibrational energy $E_{\text{vib},0}$, and the increase of the translational, vibrational, and rotational energies upon heating from 0 to 298 K, $E_{\text{trans},298}$, $E_{\text{vib},298}$, and $E_{\text{rot},298}$, respectively.

$$\Delta H_{298} = H - H^\circ = D_e + E_{\text{therm}} - (D_e^\circ + E_{\text{therm}}^\circ) + p\Delta V + \text{BSSE}$$

with

$$E_{\text{therm}} = E_{\text{vibr},0} + E_{\text{vibr},298} + E_{\text{trans},298} + E_{\text{rot},298} \quad (3)$$

Since the volume of the separate molecules is nearly identical to the volume of the complex, as judged by the sum of the van der Waals radii, the work term, $p\Delta V$, vanishes. The entropies include all translational, vibrational, and rotational contributions as well. All thermodynamics data were calculated using all vibrational modes, including soft modes below 10 cm^{-1}. Of course, in solution the distances between solute and solvent will not be as large as 330 pm and, consequently, the conformational changes of IPC during the solvation process are not well described by substantially varying the solute−solvent distances. Thus, the Gibbs free energies calculated along this particular coordinate do not yield theoretically expected relative populations in the various IPC−S complex conformations. Nevertheless, the sequence of these calculations establishes an overview of the possible structural changes. A more realistic scenario in solution is that the IPC geometry changes while the solute−solvent distance remains relatively constant. To simulate such a scenario, we constrained all bond angles in IPC to their nearly D_{3h} values calculated at a 330 pm IPC−Bz distance and subsequently recalculated the Gibbs free energy profile as we reduced the IPC−Bz distance. The Gibbs free energy profiles, ΔG_{298}, for the D_{3h} constrained and unconstrained IPC are plotted in Figure 5. In contrast to the previously calculated energy profile, this graph must be located at higher energies, as the calculations were subject to geometric constraints. The energy differences $\Delta G_{\text{conf},298}$ between the constrained and unconstrained calculations provided an energy profile that we used to estimate the Gibbs free energy reduction upon formation of an IPC−Bz complex with IPC in the C_{2v} conformation. The energy difference is defined as

$$\Delta G_{\text{conf},298} = \Delta G_{298}(\text{unconstrained}) - \Delta G_{298}(D_{3h}\ \text{constrained}) \quad (4)$$

This energy profile, depicted in Figure 5, is slightly attractive. While this profile is not an accurate representation of the energy profile for IPC−Bz complex formations, it does provide a reasonable estimate. The complex geometry continuously changes upon reduction of the IPC−Bz distance, and the sudden slope change at 240 pm coincides with the onset of substantial IPC deformation due to the interaction with a solvent molecule.

The equilibrium relative populations of the D_{3h} and C_{2v} conformers were estimated from the difference of the Gibbs free energies of both graphs at 236−250 pm, which are our best estimates for the equilibrium IPC−S distances. At these distances, ΔG_{conf} ranges from −2.5 to −2.0 kJ/mol. This corresponds to an estimated relative C_{2v} population of IPC of about 70%. The energy profile seems to suggest that the minimum intermolecular distance is below 225 pm. However, this profile represents one specific scenario that approximately quantifies the thermodynamic preference for distorting IPC into C_{2v} or C_{4v} symmetry. Consequently, we do not consider this profile a complete energetic representation of the IPC−S encounter process. Calculations that are more accurate would have to include surrounding solute molecules. Nevertheless, the estimated relative populations are in good agreement with the values experimentally obtained, as discussed in the later sections. This indicates that, in fact, calculations of just the bimolecular IPC−S complex without the surrounding solvent molecules describe the most important physical properties of the complex formation. IPC−PFBz and IPC−FBz profiles were not calculated.

We estimated the basis set superposition error using the counterpoise method.[60−62] The BSSE was calculated for two IPC−Bz separations, 330 and 250 pm. The 250 pm calculations were carried out for structurally unconstrained and D_{3h} constrained IPC, corresponding to the energy profiles depicted in

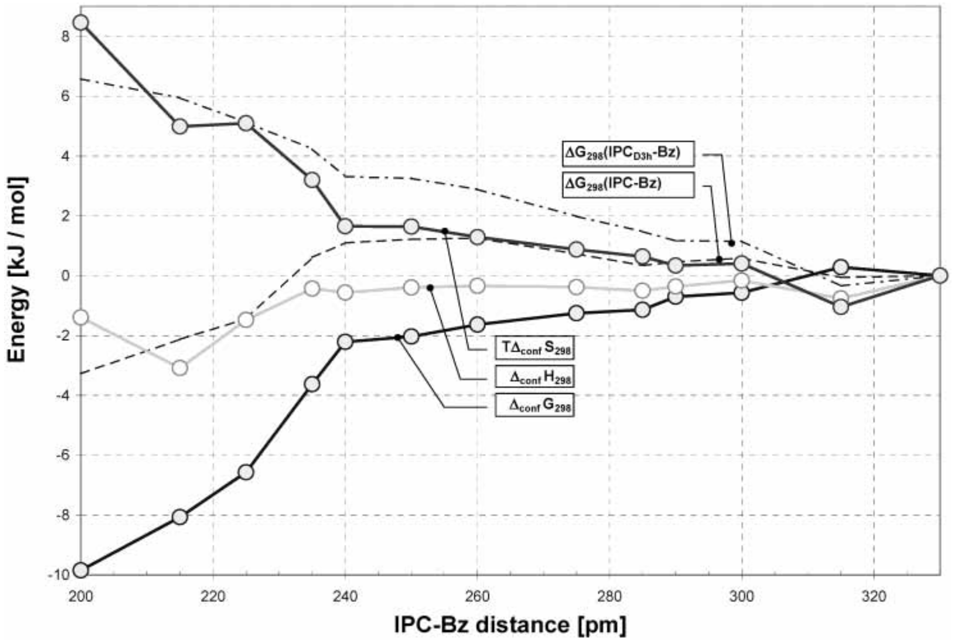

Figure 5. Gibbs free energies for various Fe(CO)$_5$−Bz distances. Representative structures of the complex are shown in Chart 1. The transformation of the Fe(CO)$_5$ from D_{3h} to C_{4v} symmetry is clearly visible. This conformational change is energetically readily accessible at room temperature. This and all other calculations were carried out with singlet IPC. This figure does not contain BSSE corrections.

TABLE 3: Calculated Energies[a] of IPC−Bz, IPC, and Bz with Different Basis Sets for the Calculation of the Basis Set Superposition Error (BSSE) Using the Counterpoise Methods[b]

	IPC−Bz (330 pm)	IPC−Bz (250 pm)	IPC−Bz (250 pm) − IPC−Bz (330 pm)	IPC_{D3_h}−Bz (250 pm)	IPC_{D3_h}−Bz (250 pm) − IPC−Bz (330 pm)
$E^{\mathrm{IPC-Bz}}_{\mathrm{IPC-Bz}}$(IPC−Bz)	$-2.421\,757 \times 10^6$	$-2.421\,733 \times 10^6$	23.68	$-2.421\,720 \times 10^6$	37.16
$E^{\mathrm{IPC}}_{\mathrm{IPC-Bz}}$(IPC)	$-1.811\,974 \times 10^6$	$-1.811\,969 \times 10^6$	4.51	$-1.811\,974 \times 10^6$	0.00
$E^{\mathrm{IPC-Bz}}_{\mathrm{IPC-Bz}}$(IPC)	$-1.811\,979 \times 10^6$	$-1.811\,976 \times 10^6$	2.11	$-1.811\,981 \times 10^6$	−2.66
$E^{\mathrm{Bz}}_{\mathrm{IPC-Bz}}$(Bz)	$-6.097\,809 \times 10^5$	$-6.097\,806 \times 10^5$	0.21	$-6.097\,794 \times 10^5$	1.47
$E_{\mathrm{IPC-Bz}}{}^{\mathrm{IPC-Bz}}$(Bz)	$-6.097\,840 \times 10^5$	$-6.097\,827 \times 10^5$	1.22	$-6.097\,837 \times 10^5$	0.21
$\mathrm{BSSE}_{\mathrm{IPC-Bz}}$[c]	8.11	9.49	1.38	12.03	3.92

[a] $E^{\mathrm{Z}}_{\mathrm{Y}}$(X) denotes the energy of system X at geometry Y with basis set Z. [b] The second, third, and fifth columns refer to the IPC−Bz complex at 330 pm, 250 pm, and D_{3h} constrained 250 pm IPC−Bz distances, respectively. The fourth and last columns contain the energy differences between the two IPC−Bz distances. All units are kJ/mol. [c]$= E^{\mathrm{IPC}}_{\mathrm{IPC-Bz}}(\mathrm{IPC}) - E^{\mathrm{IPC-Bz}}_{\mathrm{IPC-Bz}}(\mathrm{IPC}) + E^{\mathrm{Bz}}_{\mathrm{IPC-Bz}}(\mathrm{Bz}) - E^{\mathrm{IPC-Bz}}_{\mathrm{IPC-Bz}}(\mathrm{Bz})$.

Figure 5. Subsequently, we calculated ΔG_{298}(unconstrained) and ΔG_{298}(D_{3h} constrained) according to eq 2; that is, we calculated the energy difference between the IPC−Bz structures at 330 and 250 pm and between the IPC−Bz structures at 330 pm and D_{3h} constrained 250 pm, respectively. These BSSE values are +1.38 kJ/mol and +3.92 kJ/mol, respectively. The difference between these BSSE values is the correction value for $\Delta G_{\mathrm{conf,298}}$, as defined in eq 4 and depicted in Figure 5. This correction value is −2.53 kJ/mol, and consequently, at the estimated equilibrium IPC−Bz distances (236−250 pm), the BSSE-corrected $\Delta G_{\mathrm{conf,298}}$ ranges from −5.0 to −4.5 kJ/mol, which corresponds to a relative C_{2v} population of IPC of 86−88%. These theoretical values are higher than our experimentally measured values (see Table 8), which likely is a consequence of restricting our calculations to a specific reaction coordinate. Nevertheless, the theoretical data clearly confirm the exothermic formation of an IPC−Bz complex. All results are compiled in Table 3.

The semiempirical calculations do not yield very accurate energy values and IPC−Bz distances. Its calculated minimum ΔD_e value of −71 kJ/mol differs from the (not BSSE corrected) minimum DFT value of −42 kJ/mol. With 310 pm, the semiemprically calculated IPC−Bz distance of smallest D_e is too large and not in agreement with our experimental data. While these inaccuracies are expected for this level of theory, it is interesting to recognize that the semiempirical calculations yield a quite realistic visualization of the solvation structure.

For comparison, similar solvent-induced C_{4v} structures have been suggested for complexes such as Cu(H$_2$O)$_5^{2+}$. This was based on the reasoning that, in contrast to the D_{3h} geometry, C_{4v} structures enable stronger interaction between the metal center and the second hydration shell.[17] Another example of a C_{4v} geometry induced by solute−solvent interactions is Cr(CO)$_5$ in an Ar matrix.[63] The interaction energy between Cr(CO)$_5$ and argon or krypton below the basal ligands was calculated to be between 2 and 4 kcal/mol.[17]

3. Experimental Details and Results

To confirm the theoretical data, FTIR measurements of the same solute−solvent systems were performed. Fe(CO)$_5$ was purchased from Aldrich (99.999%) and used as received. The solvents were purchased from Aldrich at 99%+ purity and used after static drying with 300-pm zeolite molecular sieves provided as beads with 4−8 mesh size.[64] All chemical preparation processes were carried out in a controlled atmosphere glovebox with on-line drying and an oxygen trapping train under nitrogen atmosphere. The glovebox was illuminated with red-filtered light of low intensity to prevent any photochemical conversion. The IR absorption spectra were recorded with a Mattson Infinity

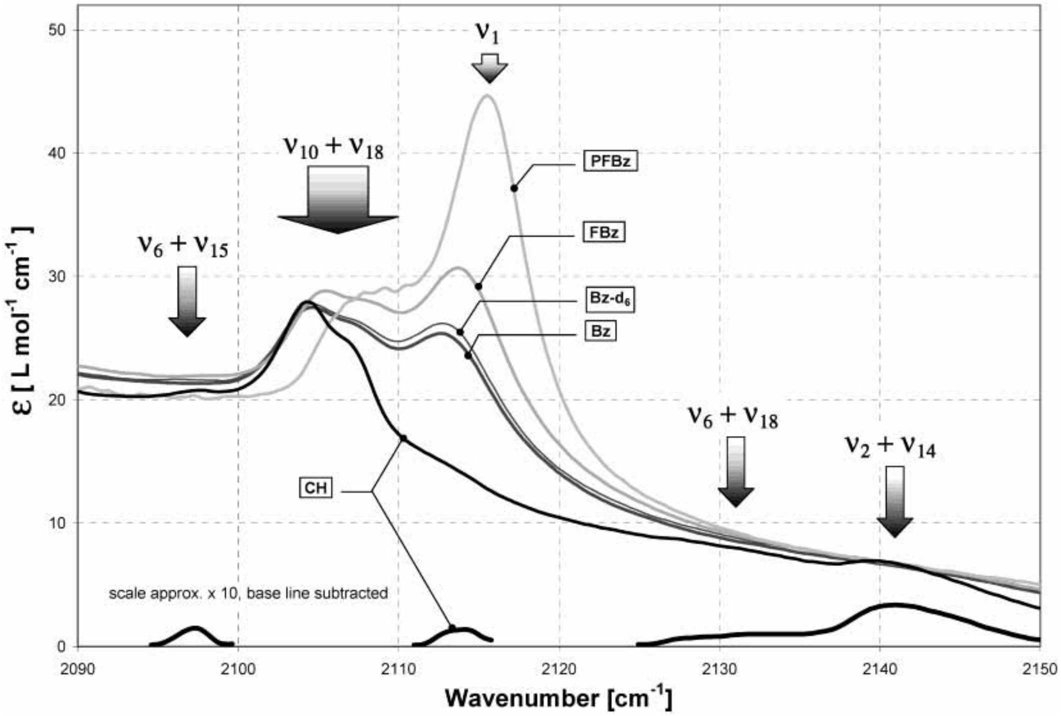

Figure 6. Measured molar absorption coefficients vs wavenumber of 100 mM iron pentacarbonyl in cyclohexane, deuterated benzene, benzene, fluorobenzene, and pentafluorobenzene.

Golden FTIR spectrometer with sample solutions of either 0.01 or 0.1 M concentration sandwiched between two CaF_2 plates. Between the windows of the IR cell a 50 μm spacer was used for the 10 mM concentration and a 500 μm spacer was used for the 100 mM concentration. Consequently, the absorbance (optical density) of the solutions could be varied by a factor of 100 with the lower absorbance being used for the measurements in the spectral range around 2000 cm^{-1}. The larger concentration used for measurements in the higher energy spectral range did not influence the shape of the measured spectra, as checked by test measurements at 10 mM concentration where the small peaks above 2100 cm^{-1} were clearly recognizable. Nevertheless, to improve the signal-to-noise ratio while maintaining the data acquisition time, the larger absorbance was chosen for this spectral range. The resolution of the FTIR spectrometer was 0.5 cm^{-1}. The spectra were fitted with Voigt profiles using the Origin Peak Fitting program, and the data listed in this paper are the results of these fits. Initially, the two intense peaks at about 2000 cm^{-1} were fitted. Subsequently, we fitted the spectrum at 2100−2200 cm^{-1}. This spectral range contains the wings of the intense, lower wavenumber peaks. To remove their contribution to the baseline, these fitted peaks were subtracted before the fitting process in the 2100 cm^{-1} spectral range. Then, we used three Voigt profiles at the positions of $\nu_{10} + \nu_{18}$, ν_1, and $\nu_2 + \nu_{14}$; see Figure 6. These procedures were applied to the sample preparation for and measurements of both solvent-dependent and temperature-dependent FTIR spectra. Afterward, the ν_1 peak areas were analyzed and yielded the conformer populations.

3.1. FTIR Measurements of the Solvent Dependence of the IPC Conformation. FTIR measurements of IPC in benzene (Bz), deuterated benzene (Bz-d_6), fluorobenzene (FBz), pentafluorobenzene (PFBz), and cyclohexane (CH) were carried out at room temperature in order to obtain the change of conformer populations in increasingly fluorinated aromatic solvents. The fitted peak areas were used as measures of the absorptions of the respective vibrational modes. Subsequently, the absorption intensities were normalized with the IR absorption strengths calculated in section 2.1.

TABLE 4: Overview over the Most Intense IR Active CO Stretching Frequencies of Iron Pentacarbonyl in Different Environments

environment	$\nu_6(A_2'')$	$\nu_{10}(E')$	ref
$Fe(CO)_5$, solid	2003	1982, 1977	43, 44
$Fe(CO)_5$, liquid	2002	1979, 1989	43
$Fe(CO)_5$, vapor	203	2013	44, 45, 48
$Fe(CO)_5$ in *n*-hexane	2022	2000	43
$Fe(CO)_5$ in CCl_4	2020	1995	44
$Fe(CO)_5$ in CS_2	2018	1995	45
$Fe(CO)_5$ in *n*-heptane	2022.9	2000.3	42
$Fe(CO)_5$ in Ar matrix	2027	2004	48
$Fe(CO)_5$ in Xe matrix	2023	1996	48
$Fe(^{13}CO)_5$, vapor	1988	1967	45
$Fe(C^{18}O)_5$, vapor	1987	1967	45
$Fe(^{13}CO)_5$ in CS_2	1973	1949	45
$Fe(C^{18}O)_5$ in CS_2	1972	1949	45
$Fe(^{13}CO)_5$, calculated	1976.8	1954.7	34
$Fe(CO)_5$, DFT calculated	2094	2067	29, 36, 65
$Fe(CO)_5$ in Bz-d_6	2020.34	1993.85	this work
$Fe(CO)_5$ in Bz	2019.97	1993.95	this work
$Fe(CO)_5$ in FBz	2021.19	1994.85	this work
$Fe(CO)_5$ in PFBz	2024.02	1997.76	this work
$Fe(CO)_5$ in CH	2021.76	1998.94	this work

Table 4 shows a compilation of the CO stretching frequencies of $Fe(CO)_5$ in different environments from both literature sources[29,34,36,37,41−45,48,65] and this work. These literature values and our measured data are in general agreement. A very detailed IR assignment of $Fe(CO)_5$ and its isotopic products in vapor and in CS_2 solution was done by Jones et al.[45] In benzene, we measured a 3 cm^{-1} blue shift for the $\nu_6(A_2'')$ mode and a 5 cm^{-1} blue shift for the $\nu_{10}(E')$ mode relative to the positions in cyclohexane. These shifts are similar to literature data for IPC in *n*-hexane, carbon tetrachloride, and carbon disulfide.[43−45] Figure 4 shows our measured IR spectra of the CO stretching modes of $Fe(CO)_5$ in different solvents. IPC in cyclohexane has narrow bands, which indicate a molecular geometry that is little influenced by solvation. The absorption bands in aromatic solvents are substantially broadened. It is a general feature of

TABLE 5: Harmonic Vibrational Frequencies of Iron Pentacarbonyl in Cyclohexane[a]

mode	symmetry	frequency (cm^{-1})	data source
ν_1	A_1'	2112	this work, directly measured, belongs to C_{4v} conformer
ν_2	A_1'	2027.9	from V. Jonas et al., ref 35
ν_6	A_2''	2022	this work, directly measured
ν_{10}	E'	1999	this work, directly measured
ν_{14}	E'	112	this work, calcd from 2140.0 cm^{-1} band minus ν_2
ν_{15}	E'	75.7	this work, calcd from 2097.7 cm^{-1} band minus ν_6
ν_{18}	E''	107	this work, calcd from 2129.0 cm^{-1} band minus ν_6

[a] Except for ν_1, all modes belong to D_{3h} symmetry.

IR spectra that upon solvation the mode frequencies red shift compared to their values in the gas phase. While this phenomenon was also observed in our measurements, we point out that the bands are increasingly blue-shifted for increasingly fluorinated solvents, suggesting increased bond strength within the CO ligands. At 100 mM concentration and 500 μm cell thickness, IR measurements in the 2100−2200 cm^{-1} region were performed. The spectra are shown in Figure 6. The corresponding data are listed in Table 6. For CH, two overlapping peaks are visible at about 2104 cm^{-1}. Jones et al.[45] interpreted peaks in this spectral range as combination modes.[45] All aromatic solvents exhibit an additional peak around 2113−2116 cm^{-1}. This peak's area increases with increasing fluorination of benzene. Simultaneously, its center shifts to higher energies. Both features, which have different, albeit related, origins, are discussed separately in the following section.

3.1.1. Change of Peak Shapes and Areas. As discussed above, $Fe(CO)_5$ in the D_{3h} configuration has two prominent IR active vibrational CO stretching modes: $\nu_6(A_2'')$ and $\nu_{10}(E')$. The E' mode is doubly degenerate and, consequently, has a larger intensity than the A_2'' mode. If the D_{3h} symmetry is broken, the degeneracy is lifted and three (overlapping) peaks are observable. In contrast, IPC with the C_{4v} configuration has three IR active modes: one doubly degenerate E mode (ν_4) and two A_1 modes (ν_1, ν_2) at higher energies.[29,34,46,50−53] Distortion of IPC with C_{4v} symmetry reduces its symmetry to C_{2v}, which causes four IR active bands: one of B_1, one of B_2, and two of A_1 symmetries. For $Fe(CO)_5$, the sum of the peak intensities of the IR absorption intensities of $\nu_6(A_2'')$ and $\nu_{10}(E')$ in D_{3h} is nearly identical to the sum of the intensities of $\nu_2(A_1)$ and $\nu_4(E)$ in C_{4v}. In fact, as shown in column 9 of Table 6, the sum of these vibrational modes remains constant for *all* symmetries and, therefore, is a measure of the total solute concentration independent of the IPC conformations. This is experimentally confirmed by the fact that the area under the peaks in the spectral range around 2000 cm^{-1} is within 2% for CH, Bz, and FBz; see Figure 4 and Table 6, column 7. Simultaneously, the appearance of the ν_1 peak for various solvents clearly proves that the distribution of IPC conformations is different in different solvents. Thus, in agreement with the theoretical spectra, the FTIR data imply that the sum of the IPC bands in the 2000 cm^{-1} spectral range does not change upon conformational change of IPC. Consequently, we used this sum to normalize the areas of other measured peaks in order to calculate relative peak areas for different solvent environments. As some peaks are related to specific IPC structures, the relative peak areas are a measure of the relative concentrations of IPC in these structures.

The peaks' centers slightly blue shift with increasing fluorination. In contrast, our calculations of isolated IPC in D_{3h} and C_{4v} are in agreement with those of Jang et al.[29] showing a red shift of these peaks. Thus, the observable vibration frequencies are shifted by the combined effects of the conformers' electronic structure changes along with nonspecific solute−solvent interactions. Nonspecific solvation potentially causes a red shift. In contrast, the details of the electronic interaction within the IPC−S complex potentially cause a blue shift. These conflicting trends are likely to be sensitively dependent on the structural details of the IPC−S complex. Since the measured spectra are superpositions of bands from structures ranging from D_{3h} to C_{4v} conformers, a substantial broadening of the modes is to be expected.

Raman active modes of $Fe(CO)_5$[43,45] exist at 2112 cm^{-1} in CS_2 solution, at 2119.5 cm^{-1} in pure liquid $Fe(CO)_5$, and at 2117 cm^{-1} in solid $Fe(CO)_5$. We assigned our measured peak at 2113 cm^{-1} to this vibration that is purely Raman active for D_{3h} symmetry. This mode is totally symmetric (A_1). Upon transformation from D_{3h} to C_{4v} structure, the mode symmetry remains A_1 but it becomes weakly IR active. Therefore, this mode becomes observable in FTIR measurements. Since a molecular symmetry change from D_{3h} to C_{2v} or C_{4v} is a prerequisite of this mode becoming IR active, the peak's area is a measure of the population in the C_{2v} and C_{4v} conformations. Assuming that the solvation process influences the respective integrated absorption coefficients to the same extent, we normalized the ν_1 peak area by the sum of the peaks areas in the range of the ν_6 and ν_{10} frequencies to obtain our desired population measure.

The peaks at about 2104 cm^{-1} were identified as a combination band consisting of $\nu_{10}(E') + \nu_{18}(E'')$ with the total symmetry $A_1'' + A_2'' + E''$. The band consists of two peaks that are clearly recognizable. The existence of this combination band is nearly independent of the conformation of IPC. For C_{4v} a corresponding combination band exists in this spectral range: $\nu_4(E) + \nu_{19}(E)$. The observed spectrum is therefore always a superposition of peaks from at least the D_{3h}, C_{2v}, and C_{4v} conformers. In contrast, the ν_1 band at 2113 cm^{-1} does not exist for the D_{3h} structure. Its position and area are strongly solvent-dependent; see Figure 6. Various other combination bands were identified, and their values were found to be in good agreement with those of Jonas et al.[35] Several vibrational frequencies for IPC in cyclohexane are compiled in Table 5. All relevant data for the peaks ν_6, ν_{10}, and ν_1 are listed in Table 6. In column 8, the peak area of ν_1 was divided by the sum of the peak areas of ν_6 and ν_{10}. This ratio, in turn, was divided by our theoretical relative IR absorption intensities (column 3, Table 7) to calculate the relative population of IPC conformers with C_{2v} symmetry; see column 5, Table 7. The equilibrium IPC−S distance for these C_{2v} conformers is listed in column 4. Only a minor IPC conformer population in aromatic solvents has D_{3h} symmetry. This population decreases as the fluorination increases. This population decrease is accompanied by a blue shift of all vibrational mode frequencies. Details of the peaks' spectral shifts will be discussed below.

In summary, the analysis presented above relied on the combined use of theoretical and experimental data. The obtained relative C_{2v} population in benzene is in good agreement with our theoretical value introduced above. These results were independently confirmed by measuring the temperature dependence of the peak area of the ν_1 mode. This analysis, presented in the following section, exclusively relied on experimental data.

3.2. FTIR Measurements of the Temperature Dependence of the IPC Conformation. The FTIR spectra at 2100−2200 cm^{-1} for IPC in benzene and pentafluorobenzene were measured

TABLE 6: Experimental IR Active CO Stretching Frequencies and Absorption Intensities of Iron Pentacarbonyl in Different Environments

IPC−S structure		M$_1$[a]	M$_2$[b]	M$_4$[c]	M$_1$/M$_2$	M$_1$ + M$_2$	M$_4$/(M$_1$ + M$_2$)
CH	frequency (cm^{-1})	1998.94	2021.76	2113.27			
	integrated absorb coeff (km/mol)	2365	1632	0.07	1.45	3997	0.002%
Bz	frequency (cm^{-1})	1993.95	2019.97	2113.27			
	int abs coeff (km/mol)	2255	1632	2.72	1.38	3887	0.070%
FBz	frequency (cm^{-1})	1994.85	2021.19	2114.03			
	int abs coeff (km/mol)	2382	1616	3.78	1.47	3998	0.094%
PFBz	frequency (cm^{-1})	1997.76	2024.02	2115.59			
	int abs coeff (km/mol)	2625	1770	5.72	1.48	4395	0.130%

[a] Peak corresponds to $\nu_{10}(D_{3h})$ and $\nu_4(C_{2v}$ and $C_{4v})$. [b] Peak corresponds to $\nu_6(D_{3h})$ and $\nu_3(C_{2v}) + \nu_2(C_{2v}$ and $C_{4v})$. [c] Peak corresponds to $\nu_1(D_{3h}$, C_{2v}, and $C_{4v})$.

TABLE 7: Relative Populations of Iron Pentacarbonyl in D_{3h} and C_{4v} or Lower Symmetry[a]

solvent	exp rel ν_1 intensity	theor rel ν_1 intensity for 100% ν_1 population	equilibirum IPC−S distance (pm)	avg C_{2v} population at avg IPC−S distance	ΔG_{conf} (kJ/mol)
CH	0.002%	0.012%	330	16.0%	4.1
Bz	0.070%	0.107%	254	65.3%	−1.6
FBz	0.094%	0.116%	248	81.4%	−3.7
PFBz	0.130%	0.132%	236	98.4%	−10.2

[a] The numbers are obtained by using FTIR results scaled by DFT calculated absorption intensities for Fe(CO)$_5$−S (S = Bz, FBz, PFBz, CH) complexes at room temperature.

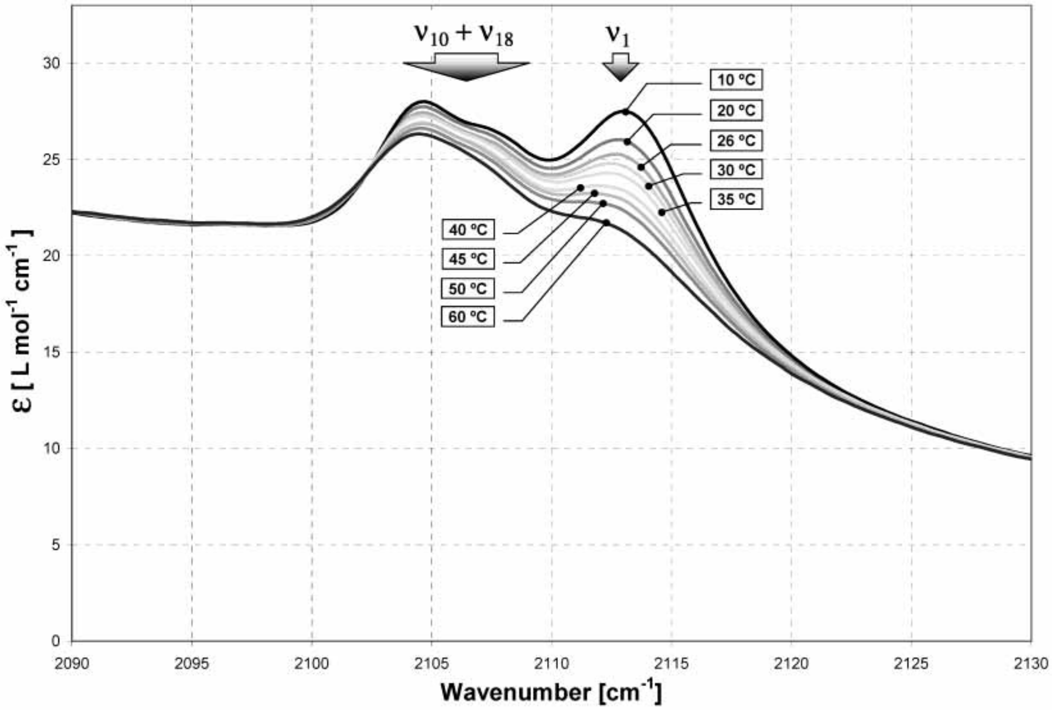

Figure 7. FTIR spectra of 100 mM iron pentacarbonyl in benzene at various temperatures.

at various temperatures in the range from −10 to 60 °C. The 500 μm cell was filled with solutions of about 100 mM concentration and mounted in a thermoelectrically controlled box within the FTIR sample chamber. We checked that the temperature distribution within this box was uniform and stable a few minutes after selecting the desired temperature. Our best estimate for the uncertainty of the temperature measurements is ±1 °C. During the measurements, the FTIR spectrometer sample chamber was flushed with dry nitrogen in order to avoid condensation. Each sequence of spectra was concluded by remeasuring the spectrum at the initial temperature in order to confirm that no chemical modifications had occurred. The essential results are presented in Figures 7 and 8, respectively. The concentrations of the C_{2v} and C_{4v} conformers relative to the total solute concentration C_{IPC} are determined by $\Delta G_{\text{conf}}(T)$, the difference of the Gibbs free energies of the D_{3h} and non-D_{3h} conformers.

$$\Delta G_{\text{conf}}(T) = -RT \ln\left(\frac{[C_{4v} + C_{2v}]}{[D_{3h}]}\right) = -RT \ln \left(\frac{[C_{4v} + C_{2v}]}{C_{\text{IPC}} - [C_{4v} + C_{2v}]}\right) \quad (5)$$

Thus, the relative concentration of the non-D_{3h} conformers is

$$\frac{[C_{4v} + C_{2v}]}{C_{\text{IPC}}} = \frac{1}{1 + e^{\Delta G_{\text{conf}}(T)/RT}} \quad (6)$$

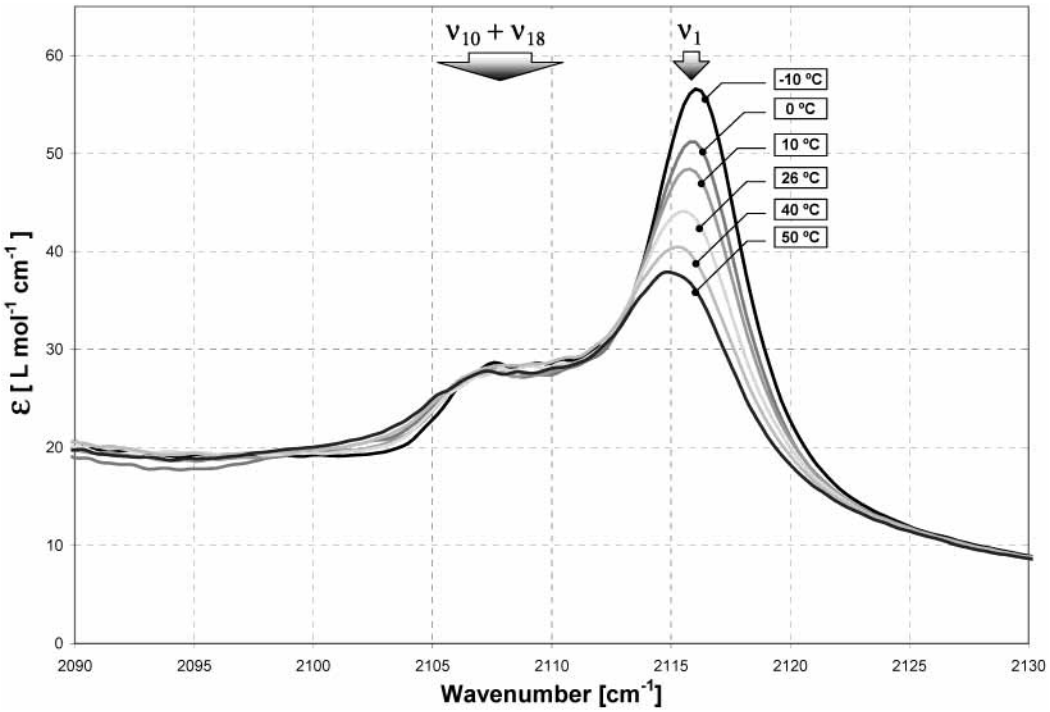

Figure 8. FTIR spectra of 100 mM iron pentacarbonyl in pentafluorobenzene at various temperatures.

We assume, as we did above, that the ν_1 peak area is proportional to the concentration of conformers in C_{4v} or lower symmetry. Thus, we define a proportionality constant c through

$$\frac{[C_{4v} + C_{2v}]}{C_{\mathrm{IPC}}}c = \frac{\mathrm{area}_{\nu_1}}{\mathrm{area}_{\nu_6+\nu_{10}}} \tag{7}$$

We then get

$$\frac{\mathrm{area}_{\nu_1}}{\mathrm{area}_{\nu_6+\nu_{10}}} = c\frac{1}{1 + \mathrm{e}^{\Delta G_{\mathrm{conf}}(T)/RT}} \tag{8}$$

ΔG_{conf} is a function of temperature. Assuming, however, that ΔH_{conf} and ΔS_{conf} are temperature independent within the temperature range used during our measurements, we write

$$\Delta G_{\mathrm{conf}}(T) = \Delta H_{\mathrm{conf}} - T\Delta S_{\mathrm{conf}} \tag{9}$$

Thus, the functional description of the temperature dependence of the ν_1 peak area contains three temperature-independent fit parameters c, ΔH_{conf}, and ΔS_{conf}. The results of the fitting procedure are listed in Table 8. The temperature-dependent relative populations are shown in Figures 9 and 10 for IPC in benzene and in pentafluorobenzene, respectively. Additionally, the measured peak shifts of the ν_1 peak are depicted. Note that these data were obtained experimentally without any input from electronic structure calculations. Yet, they are in good agreement with the populations obtained by the previous methods. Again, we find that only a minor conformer population in aromatic solvents has D_{3h} symmetry, and again, this population decreases as the fluorination increases.

TABLE 8: Thermodynamic Parameters from Fits to the Temperature Dependence of the IR Absorption Spectra with the Temperature-Dependent FTIR Results Yielding Gibbs Free Energies for Fe(CO)$_5$−Bz and Fe(CO)$_5$−PFBz Complexes[a]

	Bz	PFBz
ΔS_{conf} (J/(K mol))[b]	−46.98 ± 8.97	−35.26 ± 7.65
ΔH_{conf} (kJ/mol)[b]	−15.17 ± 3.85	−15.02 ± 2.83
data at 25 °C:		
ΔG_{conf} (kJ/mol)	−1.17	−4.50
rel population of IPC with C_{2v} symmetry	61.6%	89.4%
rel population of IPC with D_{3h} symmetry	38.4%	10.6%
ratio of populations	1.6:1	8.5:1

[a] The numbers are obtained by using the FTIR results scaled by the DFT calculated absorption intensities for Fe(CO)$_5$−S (S = Bz, FBz, PFBz, CH) complexes at room temperature. [b] Uncertainties denote 95% confidence intervals.

3.2.1. Blue Shift of Peak Centers. In general, IPC's vibrational modes red shift upon solvation through nonspecific solute−solvent interactions, such as hydrogen bonding. Generally, such shifts are temperature dependent. As temperature increases, the solution's density decreases and the average IPC−solvent distance increases. Spectral shifts induced by nonspecific IPC−solvent interactions should blue shift with increasing temperature, as for low densities the mode frequencies should approach the gas-phase limits. In contrast, we observed a blue shift upon temperature reduction, which must have been caused by the specific solvent interaction with the iron atom of IPC. Our DFT calculations showed that the blue shifts are caused by electron density shifts toward the solvent hydrogen directly interacting with the metal center of IPC. This causes a reduction of electron density of π-back-bonding orbitals within IPC. These molecular orbitals are bonding between iron and the ligands and antibonding between C and O. Consequently, a reduction of electron density in π-back-bonding orbitals causes an increase of the iron-ligand distances and a simultaneous decrease of the carbonyl bond lengths and strengths with, in turn, blue-shifted CO stretching frequencies. This explanation is consistent with the observed increasing blue shift upon increasing fluorination of the solvent, causing an increased electron density shift toward the solvent molecule. Furthermore, our DFT calculations showed that the energy profile D_e(IPC−S distance) is attractive for IPC−S distances larger than 215 pm. Thus, within the framework of this model, the observed blue shift with decreasing

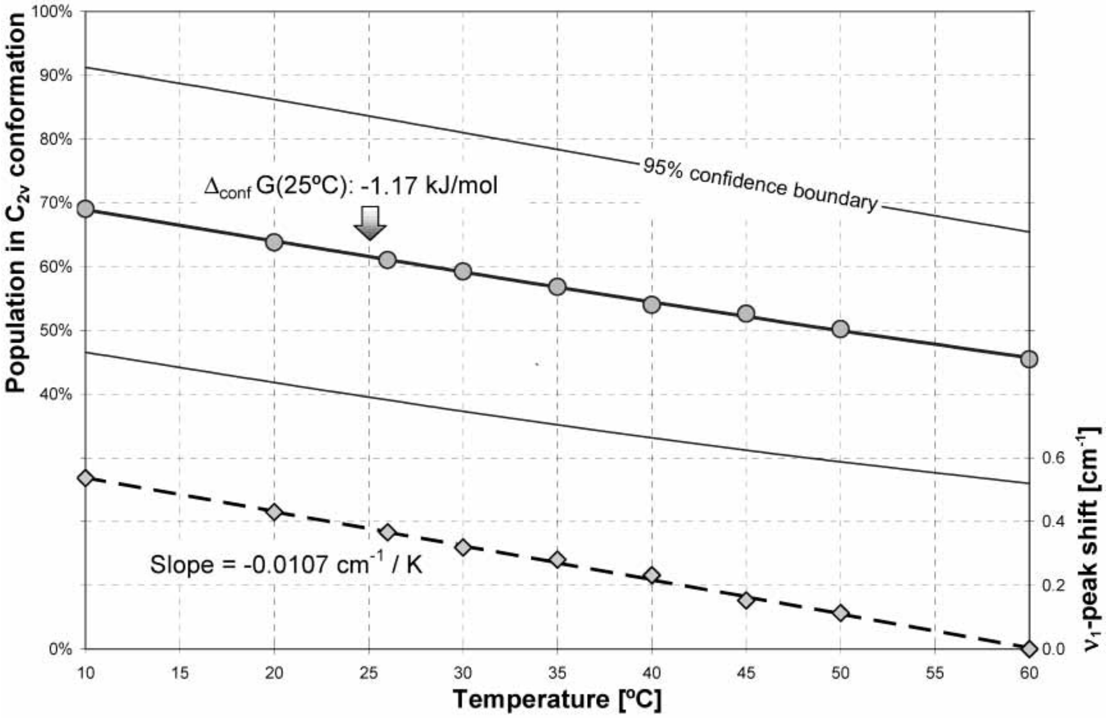

Figure 9. Experimental relative C_{2v} conformer population of IPC in benzene at various temperatures based on the spectra displayed in Figure 7.

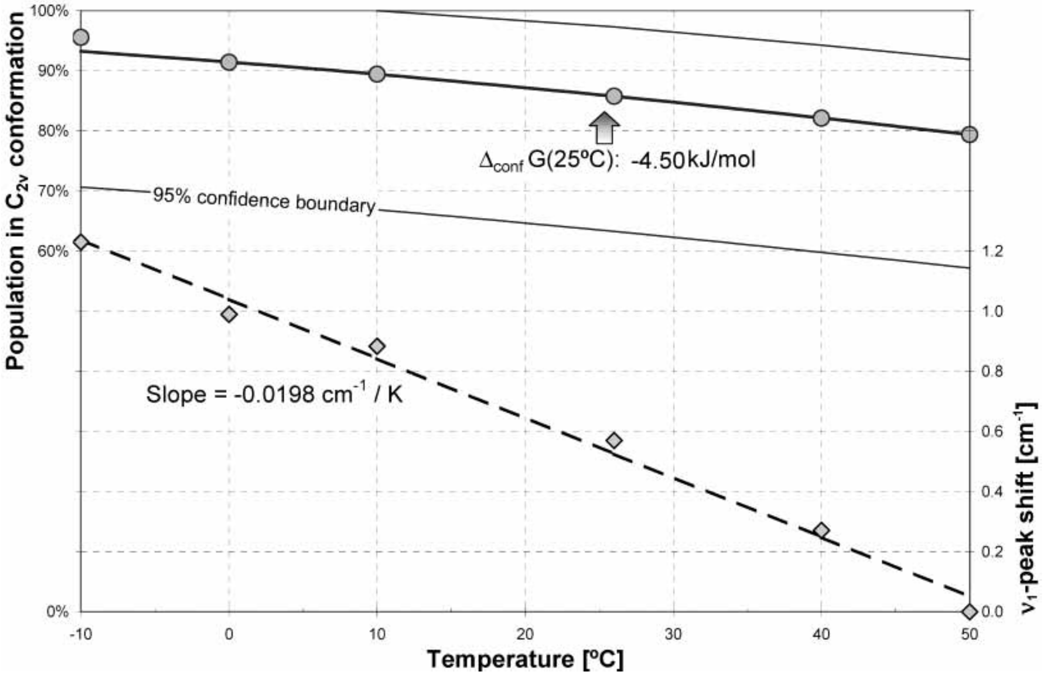

Figure 10. Experimental relative C_{2v} conformer population of IPC in pentafluorobenzene at various temperatures based on the spectra displayed in Figure 8.

temperature was caused by the decreasing equilibrium IPC−S distance, which, in turn, causes an increased electronic interaction.

The observed blue shift of the IR peaks is of diagnostic importance, as it implies the direction of the electron density shift between IPC and its associated solvent molecule. Nevertheless, we do not believe that the specific electron density shifts from IPC toward the solvent molecule are the cause of the complex formation. In fact, preliminary FTIR measurements showed that the sequence of the solvents anisol, nitrobenzene, and aniline exhibits an increasing ν_1 peak area accompanied by an increasing *red* shift of the mode frequency relative to the frequency in benzene. Thus, the formations of IPC−S complexes with C_{2v} symmetry for IPC and the spectral shifts are not necessarily caused by the same physical effect albeit they appear simultaneously. The current evidence, which is still being analyzed, indicates that the cause of the IPC−S complex formation along with its negative Gibbs free energy is the interactions between a single solvent molecule and the basal CO ligands. The interaction of the solvent molecule with the metal center of IPC seems to be a secondary effect. To test this hypothesis and the concept of an electron density shift between the solvent molecule and the IPC metal center, calculations and measurements with sterically crowded aromatics, such as mesitylene, will be carried out in the future.

4. Mechanistic Consequences and Impact on Molecular Reaction Dynamics

Structural flexibility of solvated $Fe(CO)_5$ is generally expected considering the energetic accessibility of the Berry pseudorotation. The IPC−S complex formation in aromatic solvents amounts to the stabilization of the pseudorotation transition state. This has significant mechanistic consequences, as the metal center is directly accessible to one solvent molecule. This affects the reaction dynamics, for instance, of photoinduced ligand substitution processes. It is generally assumed that such reactions for coordinatively saturated coordination complexes proceed though a dissociative mechanism. After the primary ligand dissociation, a diffusion-controlled reactive encounter of the unsaturated complex and another reactant, such as a solvent molecule, completes the substitution process, leading to the product. For the systems studied here, the encounter complex forms though a weak association of the prospective reactants before any ligand substitution process. Consequently, a ligand substitution with $Fe(CO)_5$ can proceed through a concerted mechanism with benzene binding and ligand CO dissociation occurring simultaneously. After photoexcitation of IPC in benzene, the resulting $Fe(CO)_4$−Bz product is likely vibrationally excited, and it is, therefore, conceivable that its appearance might be delayed until the excess energy has been dissipated into the solvent. However, since no diffusive reactant encounter is necessary, the product should form immediately. If the apical ligand dissociates, only an inversion of the $Fe(CO)_4$ moiety is required and a simultaneous increase of the bond strength is expected between the already associated benzene hydrogen and the iron atom. Alternatively, the ligand dissociation may proceed via pseudorotation during the S_1 to S_0 relaxation of $Fe(CO)_4$,[14−16,66] in which case the structural substitution motions would be more complicated. In any case, no diffusive reactant encounter is necessary. While $Fe(CO)_4$−Bz is not very stable under ambient conditions, it has already been proposed as a reaction intermediate by Church et al.[67] after photodissociation of $Fe(CO)_5$ solvated in benzene. The rate constant for this reaction step could not be measured. We suggest that $Fe(CO)_4$−Bz was formed on an ultrafast time scale, which we define here as a time scale faster than that of a diffusive reactant encounter. Such conclusions cannot be drawn from gas-phase studies of isolated IPC, as any coordinating reaction partner is missing and, therefore, any ligand exchange process has to be purely dissociative.

Solvated iron pentacarbonyl is a prototype for a larger class of monometallic systems, which are electronically saturated but not sterically crowded. Several such pentacoordinated neutral and ionic complexes were already mentioned above. In principle, ultrafast, nondiffusion limited, bimolecular reactions may be observable in solution if direct solvent access to the metal center is possible and appropriate conformational changes are energetically accessible. Nevertheless, despite complex formation between reactants, the dynamics might be diffusion controlled. This is, in our view, exemplified in the case of the photoinduced ligand substations reactions of $Fe(CO)_5$ in alcohols: Snee et al.[68] investigated the ultrafast reaction kinetics of photogenerated $Fe(CO)_4$ and $Cr(CO)_5$ in alcohols of varying chain lengths. They found that the reactions rates for the formation of $Cr(CO)_5OH$−R and $Fe(CO)_4OH$−R increase with the viscosities of the alcohols. While measured product formation times ranged from about 40 ps in methanol to hundreds of picoseconds in higher alcohols, the authors concluded that the values measured for methanol were too large and, in the case of $Fe(CO)_4$, no triplet intermediate was observed. Furthermore, our own calculations of $Fe(CO)_5$ in methanol yielded a structure similar to the one depicted in Figure 1 with one methyl hydrogen interacting with the iron atom. In $Fe(CO)_4OHCH_3$, however, the methanol ligand interacts with the metal center though the oxygen atom; see, for instance, Snee et al.[68] Higher alcohols are bound in the same way. Thus, upon photolysis of $Fe(CO)_5$, the associated alcohol has to rotate or another alcohol molecule has to diffusively encounter the iron center and bind. Longer chain alcohols should suffer many collisions during their reorientation processes, and for them the reorientations should proceed diffusively on viscosity-dependent time scales, as experimentally confirmed.[68] Thus, we believe that the system of IPC in higher alcohols is an example where an IPC−solvent complex is formed in solution, yet the ligand substitution time scale for large solvent molecules is still diffusion controlled. In contrast, the rotation times of small molecules certainly depend on the details of their local solvation environment. However, it has been shown that small solvent molecules can reorient during solvation processes with a large fraction of the solvation process occurring on a time scale ranging from about 100 fs for methanol[69,70] to 20 fs for water.[71] Thus, the time for the completed ligand substitution process should not be primarily influenced by the methanol rotation time but the time for CO dissociation and possible cage escape of the leaving CO group. An upper limit for this time for solvated IPC can be estimated from literature data for solvated $Cr(CO)_6$: Ligand substitution of $Cr(CO)_6$ in alcohols has to proceed purely dissociatively, followed by substantial reorganization of the intermediate, because the solute is sterically too crowded to allow for Cr−solvent coordination prior to photolysis. For instance, the formation time of $Cr(CO)_5OH$−R in methanol was measured by Simon et al.[72] to be 2.5 ps. However, these authors[73] found that the dissociation of a CO ligand was completed within 500 fs, a value that was refined to 250 fs by Joly et al.[74] These values are similar to those for gas-phase dissociation of various transition metal carbonyls.[14,75,76] Thus, as expected, the time needed for the formation of $Cr(CO)_5OH$−R is primarily determined by the solvation and reorganization of the $Cr(CO)_5$ intermediate as an incoming solvent molecule tries to associate with the metal center.[75] This is in contrast to the ligand substitution for IPC in benzene and its fluorinated derivatives but also other solvents, such as methanol. As discussed, the reaction proceeds concertedly and does not require substantial reorganization after photoexcitation, as an IPC−solvent complex already exists under equilibrium conditions. Consequently, ligand substitution reactions for IPC in these solvents should potentially proceed faster than those for $Cr(CO)_6$. As discussed for IPC solvated in aromatics, the formation of, for example, $Fe(CO)_4C_6H_6$ should be completed after CO dissociation and slight modification of the bond angles of the basal CO ligands. In methanol, the process should be just as fast, as rotation of methanol is nearly instantaneous. Thus, the literature values of a few hundred femtoseconds for the CO dissociation times of solvated $Cr(CO)_6$ should serve as a rough estimate of the upper time limit for corresponding reactions of $Fe(CO)_5$.

So far, the discussion ignored the fact that ground-state $Fe(CO)_5$ has singlet multiplicity and ground-state $Fe(CO)_4$ has triplet multiplicity. Thus, in principle, the possibility of intersystem crossing has to be considered if $^3Fe(CO)_4$ is formed en route to the final reaction product. We believe, however, that a triplet state is not involved in the ligand substitution reaction.

Gas-phase studies have demonstrated that the UV photoexcitation of IPC causes the loss of a single CO ligand within 150 fs via a conical intersection along the reaction coordinate. Further ligand dissociation occurs from the electronic ground state of the vibrationally hot $Fe(CO)_4$ on the picosecond time scale.[14−16] This rapid dissociation process makes the involvement of a triplet intermediate highly unlikely, as intersystem crossing on the 100 fs time scale cannot be expected. Moreover, the IPC−S complexation further minimizes the possibility of the involvement of any triplet state. Since the substitution process proceeds associatively/dissociatively, an isolated $Fe(CO)_4$ will never be produced, which precludes an $^3Fe(CO)_4$ intermediate. These arguments should also hold for methanol because of its IPC−methanol complex formation and its fast rotation during the substitution process. This leads us to the suggestion that the ligand substitution for $Fe(CO)_5$ in solvents that form IPC−solvent complexes under equilibrium conditions can proceed without formation of $^3Fe(CO)_4$ and can be completed on the time scale of a few vibrational periods for $Fe(CO)_5$.

In summary, the IPC−S complex formation offers important opportunities for investigations of the ultrafast dynamics of bimolecular reactions. The IPS−S association presented here could be used to photoinduce bimolecular reactions that should preserve vibrational coherence from the reactants to the products, an effect that has been observed in the gas phase for various transition metal carbonyls.[66,75] Coherent structural motions should be observable by ultrafast time-resolved optical and X-ray spectroscopic measurements. Diffusive and direct reaction pathways could be experimentally separated by varying the temperature of the solution, as this shifts the equilibrium populations between IPC(D_{3h}) and IPC(C_{2v})−S, as depicted in Figures 9 and 10.

5. Conclusion

Three methods were used to investigate the solvation structure of IPC, calculations of conformer equilibrium populations based on DFT structure calculations of the IPC−S complex, experimental FTIR data in combination with theoretical IR absorption spectra, and temperature-dependent FTIR data. All methods arrive at the same conclusion: over 60% of IPC molecules solvated in benzene and about 90% of IPC molecules in pentafluorobenzene are in the C_{2v} conformation forming an IPC−S complex. Our DFT calculations suggest that the solvent molecule approaches IPC with one of its hydrogen atoms interacting directly with the iron of IPC. The iron−hydrogen distance was determined to be about 250 pm. Since our measurements relied exclusively on FTIR methods, we were not able to directly measure changes of the iron−ligand bonds that would characterize the various IPC conformers. Our determination of the IPC−S structure is in that sense indirect and ultimately relies on the correlation of FTIR measurements with DFT calculations. However, such distances should be obtainable by X-ray absorption spectroscopic measurements of the solvation systems discussed here. We have carried out such measurements and are in the process of analyzing the data.[54,55]

Acknowledgment. We thank Dr. Dwight Sweigart for stimulating discussions, Dr. Werner Fuss for valuable comments, and Mr. Gyanprakash Ketwaroo for his contributions during the early phases of the project. The authors gratefully acknowledge partial funding and support for this work by the National Science Foundation, Grant No. CHE-9984890, and the Research Corporation, Grant No. RI0455.

References and Notes

(1) Hoye, T. R.; Suriano, J. A. *J. Am. Chem. Soc.* **1993**, *115*, 1154−6.

(2) Cheng, H.; Reiser, D. B.; Dean, S. W., Jr.; Baumert, K. *J. Phys. Chem. B* **2001**, *105*, 12547−12552.

(3) Knolker, H.-J. *Chem. Soc. Rev.* **1999**, *28*, 151−157.

(4) Suslick, K. S.; Hyeon, T.; Fang, M.; Cichowlas, A. A. *Adv. Catal. Nanostruct. Mater.* **1996**, 197−212.

(5) Wrighton, M. *Chem. Rev. (Washington, D. C.)* **1974**, *74*, 401−30.

(6) Geoffroy, G. L.; Wrighton, M. S. *Organometallic photochemistry*; Academic Press: New York, 1979.

(7) Bañares, L.; Baumert, T.; Bergt, M.; Kiefer, B.; Gerber, G. *J. Chem. Phys.* **1998**, *108*, 5799−5811.

(8) Heilweil, E. J.; Cavanagh, R. R.; Stephenson, J. C. *J. Chem. Phys.* **1988**, *89*, 230−9.

(9) Lorono, M.; Cruse, H. A.; Davies, P. B. *J. Mol. Struct.* **2000**, *519*, 199−204.

(10) Asselin, P.; Soulard, P.; Tarrago, G.; Lacome, N.; Manceron, L. *J. Chem. Phys.* **1996**, *104*, 4427−433.

(11) Lian, T.; Yang, H.; Asplund, M.; Bromberg, S. E.; Harris, C. B. Femtosecond IR studies of solvation by probing the solvent. In *Springer Series in Chemical Physics*; Toennies, J. P., Ed.; 1996; Vol. 62, pp 300−301.

(12) Joly, A. G.; Nelson, K. A. *Chem. Phys.* **1991**, *152*, 69−82.

(13) King, J. C.; Zhang, J. Z.; Schwartz, B. J.; Harris, C. B. *J. Chem. Phys.* **1993**, *99*, 7595−601.

(14) Trushin, S. A.; Fuss, W.; Kompa, K. L.; Schmid, W. E. *J. Phys. Chem. A* **2000**, *104*, 1997−2006.

(15) Ihee, H.; Cao, J.; Zewail, A. H. *Angew. Chem., Int. Ed.* **2001**, *40*, 1532−1536.

(16) Poliakoff, M.; Turner, J. J. *Angew. Chem., Int. Ed.* **2001**, *40*, 2809−2812.

(17) Demuynck, J.; Strich, A.; Veillard, A. *Nouv. J. Chim.* **1977**, *1*, 217−28.

(18) Rossi, A. R.; Hoffmann, R. *Inorg. Chem.* **1975**, *14*, 365−374.

(19) Braga, D.; Grepioni, F.; Orpen, A. G. *Organometallics* **1993**, *12*, 1481−3.

(20) Beagley, B.; Cruickshank, D. W. J.; Pinder, P. M.; Robiette, A. G.; Sheldrick, G. M. *Acta Crystallogr.* **1969**, *B25*, 737−44.

(21) Beagley, B.; Schmidling, D. G. *J. Mol. Struct.* **1974**, *22*, 466−8.

(22) Braga, D.; Grepioni, F.; Orpen, A. G. *Organometallics* **1994**, *13*, 3544−56.

(23) Cotton, F. A.; Dunne, T. G.; Wood, J. S. *Inorg. Chem.* **1965**, *4*, 318−25.

(24) Raymond, K. N.; Corfield, P. W. R.; Ibers, J. A. *Inorg. Chem.* **1968**, *7*, 1362−72.

(25) Spiro, T. G.; Terzis, A.; Raymond, K. N. *Inorg. Chem.* **1970**, *9*, 2415−20.

(26) Riedel, E. F.; Jacobson, R. A. *Inorg. Chim. Acta* **1970**, *4*, 407−11.

(27) Cramer, R. D.; Lindsey, R. V., Jr.; Prewitt, C. T.; Stolberg, U. G. *J. Am. Chem. Soc.* **1965**, *87*, 658.

(28) Blyholder, G.; Springs, J. *Inorg. Chem.* **1985**, *24*, 224−7.

(29) Jang, J. H.; Lee, J. G.; Lee, H.; Xie, Y.; Schaefer, H. F., III. *J. Phys. Chem. A* **1998**, *102*, 5298−5304.

(30) Berry, R. S. *J. Chem. Phys.* **1960**, *32*, 933−8.

(31) Spiess, H. W.; Grosescu, R.; Haeberlen, U. *Chem. Phys.* **1974**, *6*, 226−34.

(32) Apostolova, E. S.; Tikhonov, A. P.; Sendyurev, O. A. *Russ. J. Coord. Chem.* **2002**, *28*, 38−45.

(33) Tanabe, T.; Morisato, T.; Suzuki, Y.; Matsumoto, Y.; Wadayama, T.; Hatta, A. *Vibr. Spectrosc.* **1998**, *18*, 141−147.

(34) Zaera, F. *Surf. Sci.* **1991**, *255*, 280−288.

(35) Jonas, V. *J. Chem. Phys.* **1995**, *102*, 8474−8484.

(36) Gutmann, V. *Monatsh. Chem.* **1977**, *108*, 429−35.

(37) Bor, G. *Inorg. Chim. Acta* **1969**, *3*, 191−5.

(38) Bor, G. *Inorg. Chim. Acta* **1969**, *3*, 196−200.

(39) Bor, G.; Jung, G. *Inorg. Chim. Acta* **1969**, *3*, 69−73.

(40) Bor, G.; Sbrignadello, G.; Marcati, F. *J. Organomet. Chem.* **1972**, *46*, 357−68.

(41) McClelland, B. W.; Robiette, A. G.; Hedberg, L.; Hedberg, K. *Inorg. Chem.* **2001**, *40*, 1358−1362.

(42) Edgell, W. F.; Dunkle, M. P. *J. Phys. Chem.* **1964**, *68*, 452−6.

(43) Bigorgne, M. *J. Organomet. Chem.* **1970**, *24*, 211−29.

(44) Cataliotti, R.; Foffani, A.; Marchetti, L. *Inorg. Chem.* **1971**, *10*, 1594−7.

(45) Jones, L. H.; McDowell, R. S.; Goldblatt, M.; Swanson, B. I. *J. Chem. Phys.* **1972**, *57*, 2050.

(46) Haas, H.; Sheline, R. K. *J. Chem. Phys.* **1967**, *47*, 2996−3022.

(47) Edgell, W. F.; Wilson, W. E.; Summitt, R. *Spectrochim. Acta* **1963**, *19*, 863−72.

(48) Swanson, B. I.; Jones, L. H.; Ryan, R. R. *J. Mol. Spectrosc.* **1973**, *45*, 324−5.

(49) Jones, L. H.; McDowell, R. S. *Spectrochim. Acta* **1964**, *20*, 248.

(50) Adams, D. M. *Metal−Ligand and Related Vibrations: a critical survey of the Infrared and Raman spectra of metallic and organometallic compounds*; Edward Arnold Ltd.: London, 1967.

(51) Cotton, F. A.; Kraihanzel, C. S. *Inorg. Chem.* **1963**, *2*, 533.

(52) El-Sayed, M. A.; Kaesz, H. D. *J. Mol. Spectrosc.* **1962**, *9*, 310.

(53) Farona, M. F.; Cutcliffe, A. B. *Spectrosc. Lett.* **1970**, *3*, 89−92.

(54) *Ultrafast laboratory-based X-ray sources and their applications in chemical research*; Lee, T., Jiang, Y., Benesch, F., Rose-Petruck, C., Eds.; SPIE Publishing: Bellingham, WA, and San Jose, CA, 2003; Vol. 4978, in press.

(55) Lee, T.; Benesch, F.; Jiang, Y.; Song, N.; Rose-Petruck, C. Submitted to *Chem. Phys.*

(56) *Ultrafast X-ray Absorption Spectroscopy: Observing the equilibrium structure and structural dynamics of solvated molecules*; Jiang, Y., Li, W., Lee, T., Ketwaroo, G., Rose-Petruck, C., Eds.; SPIE Publishing: Bellingham, WA, 2001; Vol. 4504, pp 42−48.

(57) Jiang, Y.; Lee, T.; Li, W.; Ketwaroo, G.; Rose-Petruck, C. *Opt. Lett.* **2001**, *27*, 963−65.

(58) Jiang, Y.; Lee, T.; Rose-Petruck, C. *J. Opt. Soc. Am. B* **2003**, *20*, 229−237.

(59) *Jaguar 3.5*; Schrodinger, Inc.: Portland, OR, 1998.

(60) Gutowski, M.; Van Lenthe, J. H.; Verbeek, J.; Van Duijneveldt, F. B.; Chalasinski, G. *Chem. Phys. Lett.* **1986**, *124*, 370−5.

(61) van Duijneveldt, F. B.; van Duijneveldt-van de Rijdt, J. G. C. M.; van Lenthe, J. H. *Chem. Rev.* (*Washington, D. C.*) **1994**, *94*, 1873−85.

(62) Rayon, V. M.; Sordo, J. A. *Theor. Chem. Acc.* **1998**, *99*, 68−70.

(63) Perutz, R. N.; Turner, J. J. *J. Am. Chem. Soc.* **1975**, *97*, 4791−800.

(64) Reichardt, C. *Solvents and Solvent Effects in Organic Chemisrty*, 2 ed.; VCH: New York, 1990.

(65) Jonas, D. M.; Bradforth, S. E.; Passino, S. A.; Fleming, G. R. *J. Phys. Chem.* **1995**, *99*, 2594−2608.

(66) Trushin, S. A.; Fuss, W.; Schmid, W. E. *Chem. Phys.* **2000**, *259*, 313−330.

(67) Church, S. P.; Grevels, F. W.; Hermann, H.; Kelly, J. M.; Klotzbuecher, W. E.; Schaffner, K. *J. Chem. Soc., Chem. Commun.* **1985**, 594−6.

(68) Snee, P. T.; Payne, C. K.; Mebane, S. D.; Kotz, K. T.; Harris, C. B. *J. Am. Chem. Soc.* **2001**, *123*, 6909−6915.

(69) Rosenthal, S. J.; Jimenez, R.; Fleming, G. R.; Kumar, P. V.; Maroncelli, M. *J. Mol. Liq.* **1994**, *60*, 25−56.

(70) Fonseca, T.; Ladanyi, B. M. *J. Mol. Liq.* **1994**, *60*, 1−24.

(71) Jimenez, R.; Fleming, G. R.; Kumar, P. V.; Maroncelli, M. *Nature (London)* **1994**, *369*, 471−3.

(72) Simon, J. D.; Xie, X. *J. Phys. Chem.* **1986**, *90*, 6751−3.

(73) Xie, X.; Simon, J. D. *J. Am. Chem. Soc.* **1990**, *112*, 1130−6.

(74) Joly, A. G.; Nelson, K. A. *J. Phys. Chem.* **1989**, *93*, 2876−2878.

(75) Trushin, S. A.; Fuss, W.; Schmid, W. E.; Kompa, K. L. *J. Phys. Chem. A* **1998**, *102*, 4129−4137.

(76) Banares, L.; Baumert, T.; Bergt, M.; Kiefer, B.; Gerber, G. *J. Chem. Phys.* **1998**, *108*, 5799−5811.